CrystEngComm

Accepted Manuscript

ROYAL SOCIETY OF CHEMISTRY

www.rsc.org/crystengcomm

Sustainable processing of waste polypropylene to produce high yield valuable Fe/carbon nanotube nanocomposites

Junhao Zhang[1, 3], Longmei Zhang[1], Huan Yang[2], Qinghong Kong[2,*], Yuanjun Liu[1], Aihua Yuan[1,*]

[1]*School of Biological and Chemical Engineering; Jiangsu University of Science and Technology; Zhenjiang Jiangsu 212018, China*

[2]*School of the Environment and Safety Engineering, Jiangsu University, Zhenjiang, Jiangsu 212013, China*

[3]*CAS Key Laboratory of Materials for Energy Conversion, University of Science and Technology of China, Hefei Anhui 230026, China*

AUTHOR INFORMATION

Corresponding Author

*Tel: +86-511-84401181. Fax: +86-511-84407381.

Email: kongqh@mail.ujs.edu.cn, aihua.yuan@just.edu.cn

Notes

The authors declare no competing financial interest.

ABSTRACT: With the increasingly serious environment contamination and energy crisis, it is very necessary that the polyolefin-based waste plastics were converted into valuable materials by innovative upcycling processes. This study presents an environmentally benign and solvent-free autogenic process to produce sponge-like Fe/carbon nanotube nanocomposites by catalytic pyrolysis of waste polypropylene (PP) at 600 °C. The composition and morphology of the products were characterized by powder X-ray diffraction (XRD), Raman spectra, X-ray photoelectron spectra (XPS), field-emission scanning electron microscopy (FESEM), and transmission electron microscope (TEM). The results show that the products are Fe/carbon nanotube nanocomposites with sponge-like structures, and the diameter of carbon nanotubes is about 30 nm and the diameter of Fe nanoparticles in carbon nanotubes is also about 30 nm, which illustrates that the size of Fe nanoparticles determines the diameter of carbon nanotubes. Nitrogen adsorption-desorption measurement indicate that the Brunauer-Emett-Teller (BET) surface area is calculated to be 197.6 m^2/g, and the Barrett-Joyner- Halenda (BJH) adsorption cumulative volume of pores is up to 0.2860 cm^3/g. The magnetic measurement at room temperature indicates that the values of saturation magnetization (62.7 emu/g) and coercivity (187.3 Oe) of the sponge-like Fe/carbon nanotube nanocomposites are different from those of bulk Fe due to the wide existence of carbon nanotubes and small size of the Fe nanoparticles.

1. Introduction

In the last years, increasing attentions are being focused on carbon encapsulated magnetic nanostructures, which contain two components: the magnetic core/filler and the non-magnetic carbon matrix/shell [1, 2]. Due to its good chemical thermal stability, carbon layer could act as a protective barrier to avoid oxidation and degradation of magnetic performance of metallic particles in harsh environments such as acidic or basic media, but also reduce the magnetic coupling between individual particles to inhibit agglomeration. Additionally, carbon has good hydrophilic and biocompatible properties, which makes it possible to load other functional molecules. Therefore, carbon encapsulated magnetic nanoparticles are promising candidates for applications in magnetic resonance imaging (MRI) [3], ultrahigh-density magnetic recording media [4], integrated diagnosis and therapeutics [5], drug delivery [6], catalysis [7], environmental protection [8], and electromagnetic (EM) wave absorption [9], etc.

Up to now, numerous techniques have been developed to synthesize carbon-encapsulated magnetic nanoparticles [10-15]. Cai prepared carbon encapsulated Fe_3O_4 nanoparticles by first introducing amorphous carbon coat on Fe_3O_4 surface with hydrothermal method and then heating the as-prepared nanoparticles in N_2 atmosphere [16]. Tsutomu synthesized onion-like carbon encapsulated Co, Ni, and Fe magnetic nanoparticles by a pulsed plasma in a liquid [17]. Zhao reported that ordered mesoporous Fe_2O_3@C encapsulates with novel nanoarchitectures have been designed and fabricated by an ammonia-atmosphere pre-hydrolysis post-synthetic route [18]. Bystrzejewski reported that carbon encapsulated iron nanoparticles were produced by carbon arc discharge [19]. Oh prepared magnetic particle-embedded porous carbon composites by one-step pyrolysis of metal-organic framework [20]. However, it is still a great challenge to develop simple,

green and economical synthetic strategies for carbon-encapsulated magnetic nanoparticles with designed chemical components and controlled morphologies.

Recently, the disposal of waste plastics has been also an important concern for the society because of the high use of different plastic polymers [21-24]. To reduce the impact of plastics on the environment, it is very necessary to design and facilitate the means of recycling more, and typically, waste reduction, recycling (mechanical, chemical, and thermal) as well as landfilling are considered as common solution. Since plastics are not biodegradable, it's not an effective solution to deal with them in landfills. The most usual alternative for the treatment of waste plastics in many countries is incineration accompanied by energy recovery [25]. This option is often socially rejected because of the risk of toxic compound emission, such as dioxins and furans. Nowadays, extensive collection, transportation, separation, and recycling facilities are available for processing waste thermoplastic products. Unfortunately, by mixing different waste plastics, homogeneous materials might not be obtained being suitable for making quality products. The problem of mixed plastics has been partially solved by separation technologies such as flotation [26], plasma gasification technology [27], and so on. However, these multistep recycling processes are not cost-effective.

Among the different alternatives for plastic waste treatment, the most promising one seems to be chemical recycling with the lowest environmental impact and the highest possible profitability. There has been recent interest in applying the technology for gasification of waste plastics to yield smaller molecules, usually liquids or gases, that are suitable as feedstocks to produce new petrochemicals and plastics. However, it requires the construction of large plants to be profitable, the processes need high reaction temperature which is more than 600 °C and even up to 900 °C [28-30], and the products are broad range. Due to the fact that carbon is the major constituent of

plastics, waste plastics can therefore provide carbon source for producing value-added carbon-based products. For example, Kartel et al.[31] prepared activated carbon with BET surface area of 1030 m^2/g and an effective pore size of 1.8 nm using polyethylene terephthalate as carbon source at 800 °C. However, the yield of solid carbon was only 22%. Williams et al.[32] reported that hydrogen and high-value carbon nanotubes were derived from waste plastic using a pyrolysis-reforming technology. The results show that around 94.4 mmol H_2 g^{-1} plastic was obtained for the pyrolysis-reforming of HDPE waste in the presence of the Ni-Mn-Al catalyst and steam at 800 °C, and about 33.8 wt.% filamentous carbon was prepared from the pyrolysis of motor oil containers in the presence of the Ni-Mn-Al catalyst without steam at 800 °C. Recently, a simple one-step process without solvents was used to convert PE and other waste plastics (such as polyethylene terephthalate, polypropylene and polystyrene) into carbon materials [33-37]. This approach is efficient and scalable, but the reaction temperatures are high and the yields are low. From the viewpoint of economically applicable process in industry, it's necessary to improve the production yield of solid carbon under mild conditions. To the best of our knowledge, few documents report the synthesis of Fe/carbon nanocomposites using waste plastics as feedstocks. As a result, converting waste plastics to Fe/carbon nanocomposites on a large scale still remains a great challenge at relative low temperature.

Herein, we introduce a creative method to convert waste PP to sponge-like Fe/carbon nanotube nanocomposites by manipulating the formation of carbon deposition on the catalyst. The process involves thermal decomposition of waste polypropylene with the presence of catalysts at 600 °C in closed reactor, which is simple, reproducible and affordable. The composition, morphology, and structure of the as obtained Fe/carbon nanotube nanocomposites are characterized

using advanced structural, spectroscopic, and imaging techniques. This invention presents an opportunity to use waste plastics as raw material for the production of Fe/carbon nanotube nanocomposites. The unique properties of Fe/carbon nanotube nanocomposites will undoubtedly have many applications in the areas of electronics, biosensors, energy storage and reinforced composites for aeroplanes, ect.

2. Experimental Section

In a typical procedure, waste PP (1.0 g), ferrocene (1.0 g) and NaN_3 (1.0 g) were loaded into a 20 mL stainless steel autoclave. The autoclave was tightly sealed and heated in an electronic furnace. The temperature of furnace was increased to 600 °C in 60 min and maintained at 600 °C for 12 h. Then, the autoclave was cooled to room temperature naturally. It was found that the final products in the autoclave were black precipitates and residual gases. The black precipitates were collected and washed with distilled water and ethanol for several times. After that, the products were dried in a vacuum box at 50 °C for 4 h, and collected for characterization.

The as-prepared products were characterized by powder X-ray diffraction (XRD) employing a Rigaku (Japan) D/max-γA X-ray diffractometer equipped with graphite-monochromatized Cu Kα radiation (λ=1.54178 Å). The Raman spectra were recorded at ambient temperature on a SPEX 1403 spectrometer with an argon-ion laser at an excitation wavelength of 514.5 nm. X-ray photoelectron spectroscopy (XPS) of the products was performed using a VGESCALABMK X-ray photoelectron spectrometer and non-monochromated Mg *Kα* radiation as the excitation source. The field-emission scanning electron microscopy (FESEM) images of the products were taken by using a field-emission scanning electron microscope (JEOL-6300F). The transmission electron microscope (TEM) images were taken on a JEOL 2010 high-resolution transmission electron microscope at an acceleration

voltage of 200 kV. Element dispersive spectrometric (EDS) analysis was carried out on an X-ray energy spectrum instrument equipped with INCA300 (Oxford). The nitrogen adsorption-desorption isotherms and textural properties were determined by Beckman Coulter SA3100. The magnetic properties (*M-H* curve) were measured at room temperature on an MPMS XL magnetometer made in Quantum Design Corporation.

3. Results and discussion

To ascertain the components and structures of the products, XRD was used to investigate the crystal phases. Fig. 1 shows the powder XRD pattern of the resulting Fe/carbon nanotube nanocomposites by catalytic pyrolysis of waste PP at 600 °C. The sharp diffraction peaks with relative high peak intensity can be well indexed as α-Fe, in agreement with the literature values (Joint Committee on Powder diffraction Standards (JCPDS), Card No. 85-1410). Meanwhile, the broad peak located at about 26.2^{o} can be assigned as amorphous graphite. No other impurity peaks were detected, revealing the high purity of the synthesized products.

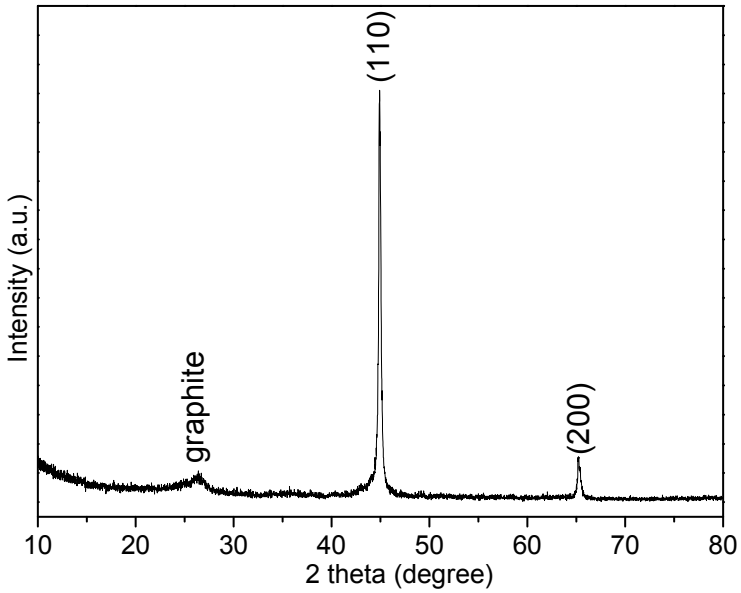

Fig. 1 A typical XRD pattern of Fe/carbon nanotube nanocomposites at 600 °C.

Raman spectrum can be used to characterize carbon structures of carbonaceous materials such as graphite and diamond-like carbon, and provides information on the molecular structure and chemical bonding of carbon atoms in carbonized materials. Fig. 2 gives their corresponding Raman spectra, showing two similar Raman bands at 1346 cm^{-1} (D band) and 1596 cm^{-1} (G band). More specifically, the two peaks exhibit an E_{2g} mode of graphite related to the vibration of sp^2-bonded carbon atoms in a 2D hexagonal lattice (such as in a graphene layer) and A_{1g} mode of graphite related to the disorder features due to the finite particle size effect or lattice distortion of the graphite crystals. The relative intensity ratio of the *D*-*G* band, I_D/I_G, can give reliable information for the graphitization degree. It is found that the Fe/carbon nanotube nanocomposites have a higher I_D/I_G, implying a highly disordered graphitic structure for carbon nanotubes, and these results are consistent with the XRD pattern.

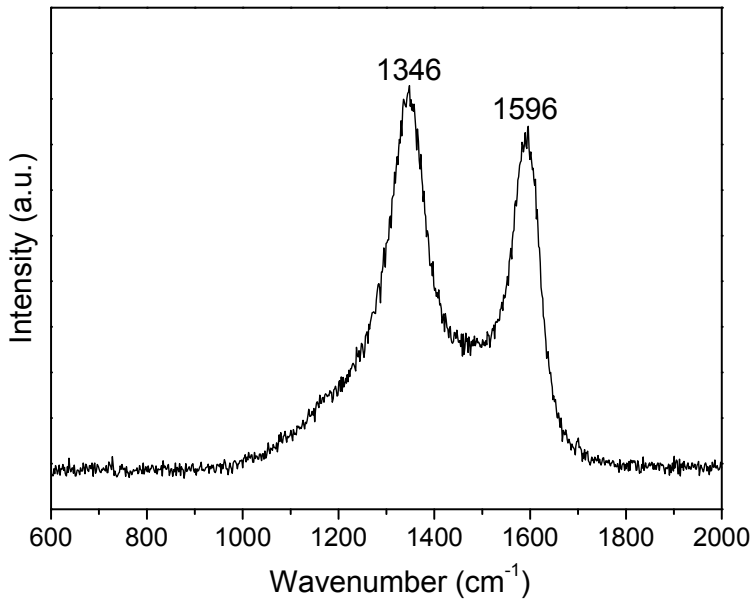

Fig. 2 Raman spectra of Fe/carbon nanotube nanocomposites at 600 °C.

X-ray photoelectron spectra (XPS) have often been used for the surface characterization of various materials, and unambiguous results are readily obtained when the various surface components each contain unique elemental markers. Here, in order to analyze the surface component

of the Fe/carbon nanotube nanocomposites, XPS of the products was measured. The XPS spectra of Fe/carbon nanotube nanocomposites are shown in Fig. 3. It can be found that the peaks on the full pattern are mainly attributed to C1s (285.7 eV), Fe2p (711.0 and 724.8 eV) and their corresponding Auger peaks in Fig. 3a. However, there are almost no peaks for the O1s binding energy detected, suggesting that the products consist of C and Fe elements. Fig. 3b shows that the peaks of Fe2p are weak, which indicates that the Fe nanoparticles maybe encapsulated in carbon.

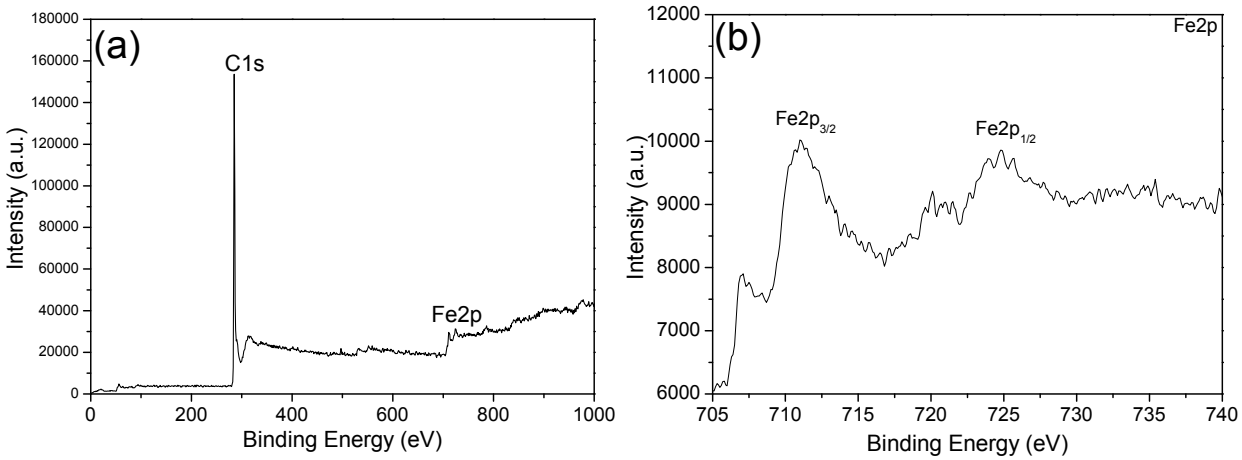

Fig. 3 X-ray photoelectron spectra of Fe/carbon nanotube nanocomposites by catalytic pyrolysis of waste PP at 600 °C: (a) a wide scan spectrum; (b) high-resolution XPS spectrum of Fe 2p region.

Magnetic materials encapsulated in carbon based systems have attracted increasing attention due to their electric and magnetic properties and their variety of potential technological application. In recent years, there have been a number of studies of iron and carbon composites. In Fig. 4a, another type of Fe/carbon nanocomposites is presented in high morphological yield, and the nanocomposites are sponge-like structures. The high magnification FESEM image in Fig. 4b shows that the nanocomposites are assembled by one-dimensional structures with diameters of about 30 nm and lengths of several micrometers. Careful observation shows that there are many catalyst nanoparticles at the tops of one-dimensional structures. The structures were further characterized by

TEM. Fig. 5a shows a TEM image of the products, which agrees with the above FESEM images. A notable result is that the diameter of carbon nanotubes is about 30 nm and the diameter of the catalyst nanoparticles is also about 30 nm, which indicates that the size of the Fe nanoparticles determines the diameter of carbon nanotubes. Fig. 5b shows that the products include some amorphous mesoporous carbon besides carbon nanotubes. From the results of TEM images, the carbon nanotubes are bamboo-like structures. The inset image in Fig. 5(b) is the SAED pattern of Fe nanoparticles which suggests that these Fe nanoparticles have body centered cubic (bcc) crystal structures. Fig. 5c is a HRTEM image for the wall structures of carbon nanotubes, which displays clear lattice fringes. The interlayer spacings in the walls are about 0.34 nm corresponding to the (002) distance of graphitic carbon lattice. However, the lattice fringes are short-range order, and the carbon nanotubes have some stacking faults, which indicate that the carbon nanotubes are low crystallinity. The results of EDS (Fig. 3d) confirm that Fe and C elements are presented in the nanocomposites. The signals of Cu element come from the supporting TEM grid during measurements.

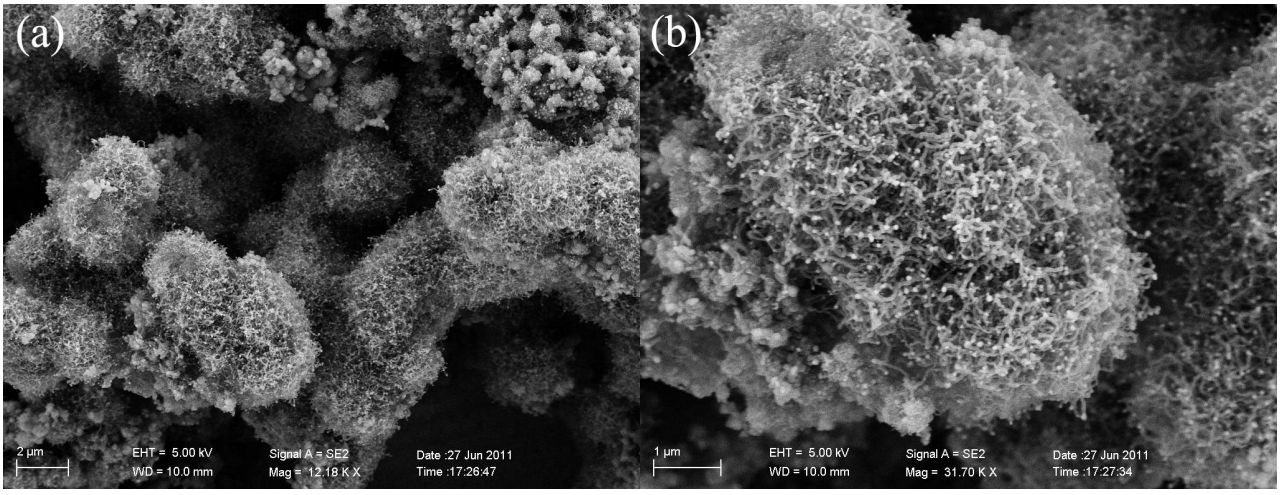

Fig. 4 (a) Low magnification FESEM image of Fe/carbon nanotube nanocomposites; (b) high magnification FESEM image of Fe/carbon nanotube nanocomposites.

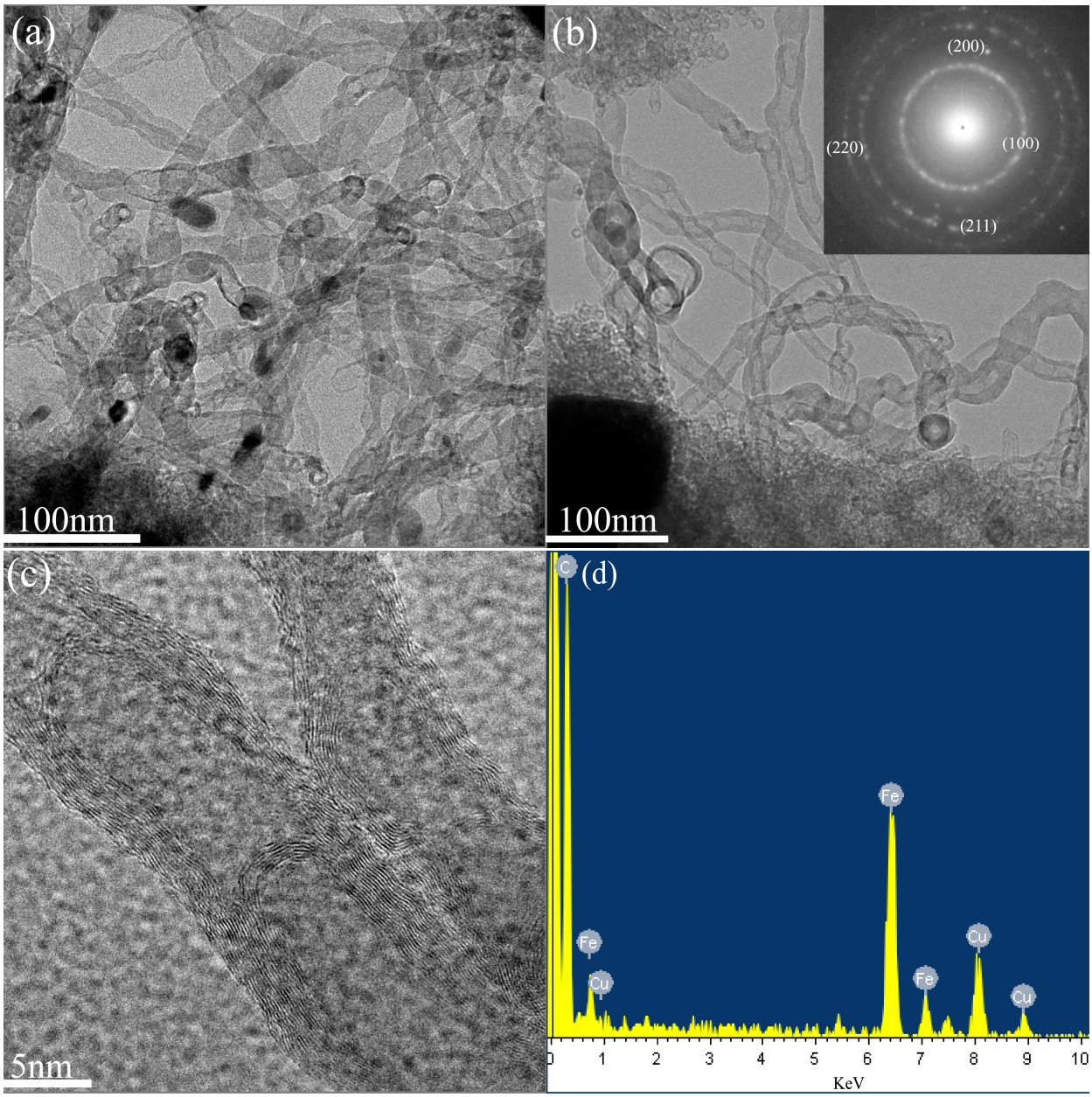

Fig. 5 (a) and (b) TEM images of Fe/carbon nanotube nanocomposites and SAED pattern of Fe nanoparticles (inset in (b)); (c) TEM image of Fe/carbon nanotube nanocomposites; (d) EDS of spectrum of Fe/carbon nanotube nanocomposites.

Nitrogen adsorption-desorption isotherms of Fe/carbon nanotube nanocomposites at 600 °C show a type IV curve in Fig. 6a. The pore size distribution derived from the adsorption branch using the BJH method shows that the pore size is centered at about 2.3, 3.4 and 30.1 nm in Fig. 6b. The BET surface area is calculated to be 197.6 m^2/g, and the BJH adsorption cumulative volume of pores is up to 0.2860 cm^3/g between 1.7 and 300 nm. This value is high comparing with that of carbon

nanotubes in our previous report [38]. According to the morphology and structure characteristic, the higher BET surface area can be attributed to the smaller diameters, rough surface and more defects of carbon nanotubes, and the existence of some amorphous mesoporous carbon.

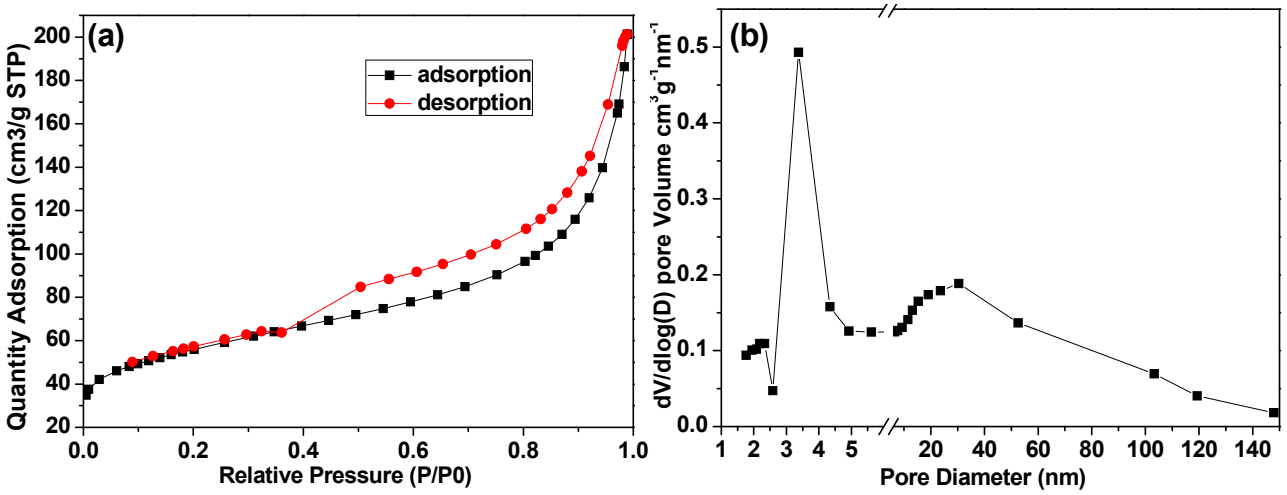

Fig. 6 (a) Typical N_2 adsorption-desorption isotherm of Fe/carbon nanotube nanocomposites at 600 °C; (b) pore size distribution of Fe/carbon nanotube nanocomposites at 600 °C.

To understand the possible formation process of the Fe/carbon nanotube nanocomposites, a series of relevant experiments were carried out by altering the experimental parameters. It is obvious that the reaction temperature plays a critical role in the formation of Fe/carbon nanotube nanocomposites. At a reaction temperature of 600 °C, the products are sponge-like Fe/carbon nanotube nanocomposites with high morphological yield. Fig. 7 shows FESEM images of the products obtained at 500 °C and 700 °C. Fig. 7(a) shows that the morphology and size of the main products are uniform for a reaction temperature of 500 °C, which are similar to sponge-like structures in Fig. 4(a), and the morphology yield is about 80%. Fig. 7(b) indicates that the products also consist of some particles and scattered carbon nanotubes. By increasing the reaction temperature to 700 °C, Fig. 7(c) shows that the products are main uniform particles, which size is the range of 200-700 nm. Careful observation shows that a small amount of carbon nanotubes are in the products,

and the high magnification FESEM image shows in Fig, 7(d). Apart from the reaction temperature, the products can also be tuned by varying reaction atmosphere. From the results of Fig.8 and Fig.9, it is found that the reaction atmosphere influence the compositions and morphologies. When H_2O was used to replace NaN_3, the products are one-dimensional and worm-like structures with the diameter of about 580 nm, and some carbon spheres with 1.7 μm are also found in the products, shown in Fig. 8(a). Fig. 9a indicates the products are the composites of C and Fe_3O_4. In this system, PP decomposed to produce small molecules carbonyl compounds as carbon source in the absence of oxygen, and Fe atoms were released by decomposition of ferrocene to act as dehydrogenation catalyst. As-formed Fe atoms reacted with H_2O to form Fe_3O_4 nanoparticles due to the presence of water vapor, and the obtained Fe_3O_4 particles were self-assembled to chain-like structures under the drive of magnetic dipole interaction. The small molecules carbonyl compounds were carbonized to produce carbon atoms, which precipitated on the surface of Fe_3O_4 chains to form worm-like structures. When $NaNH_2$ was used to replace NaN_3, the products are nanoflakes and nanoparticles and mainly composed of C and Fe, shown in Fig. 8(b) and Fig. 9(b). The formation mechanism is similar to that of using NaN_3. If $NaNH_2$ replaces NaN_3, $NaNH_2$ decompose to release Na, N_2, H_2 and NH_3. Fe atoms were not oxidized in the presence of Na and H_2, which acted as dehydrogenation catalyst to decompose small molecules carbonyl compounds to form carbon atoms. Carbon atoms were promoted to deposit on the surface of Fe nanoparticles and form a thin carbon lamella which reduced the surface energy and prevented the continued growth of Fe nanoparticles. As carbon atoms are enough in the system, the redundant carbon atoms lead to the formation of carbon nanoflakes. When NaN_3 was replaced by $CO(NH_2)_2$, the products are large amounts of flower-like structures assembled by nanoflakes and nanoparticles and mainly composed of C and Fe_3O_4, shown in Fig. 8(c)

and Fig. 9(c). In this process, the obtained Fe atoms were oxidized to form Fe_3O_4 particles in the atmosphere of NH_3 and HCNO by decomposition of $CO(NH_2)_2$. The formation process of the products is similar to that of $NaNH_2$. When NaN_3 was replaced by S powder, Fig. 8d displays that the products include flower-like spheres, big flake and polyhedron structures. Fig. 9d reveals that the products are the composites of C and FeS. In this process, Fe atoms reacted with S to form FeS particles. Carbon atoms from catalytic carbonization of PP were precipitated to form carbon flakes and flower-like spheres. Consequently, it can be believed that appropriate atmosphere could facilitate the assembly of sponge-like Fe/carbon nanotube nanocomposites.

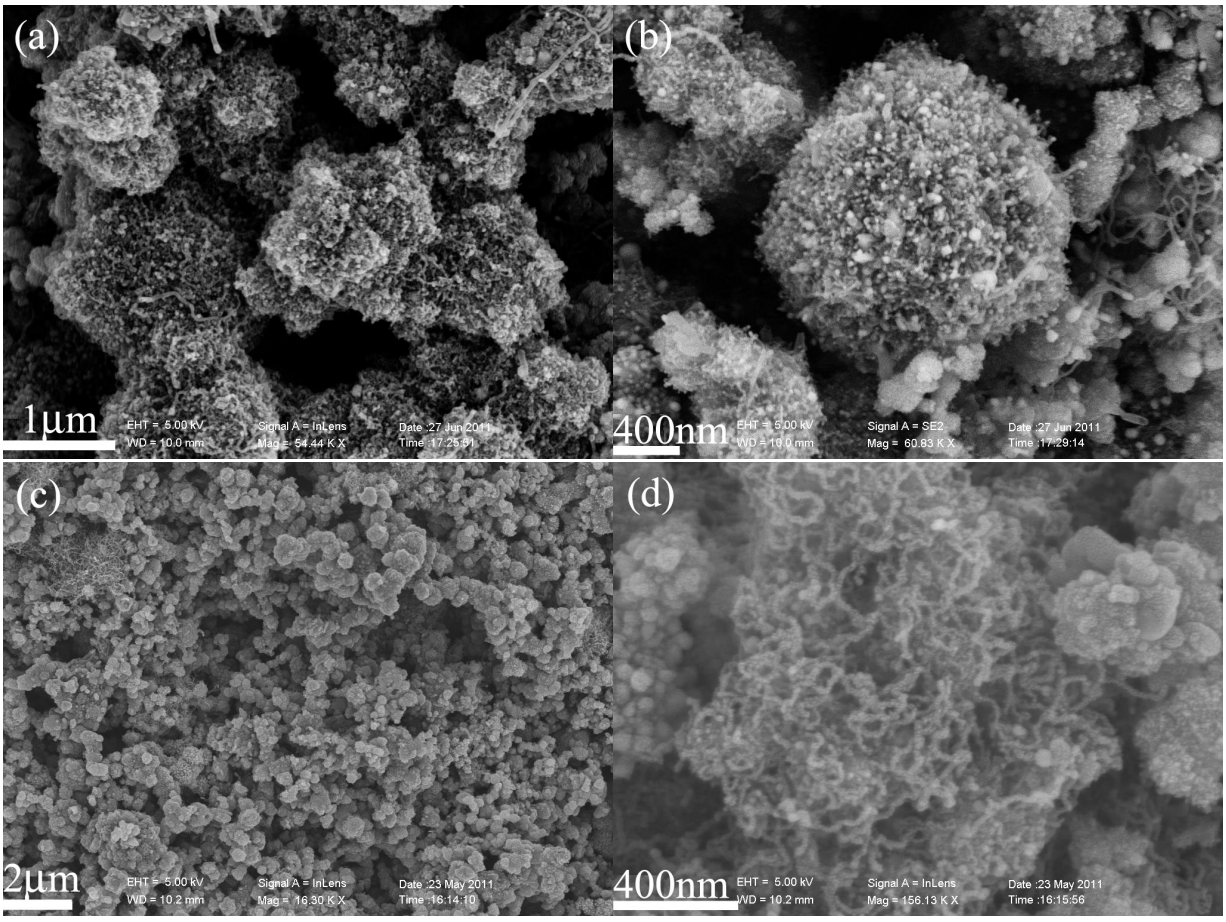

Fig. 7 (a) Low magnification FESEM image of the products obtained at 500 °C; (b) high magnification FESEM image of the products obtained at 500 °C; (c) low magnification FESEM image of the products obtained at 700 °C; (d) high magnification FESEM image of the products obtained at 700 °C.

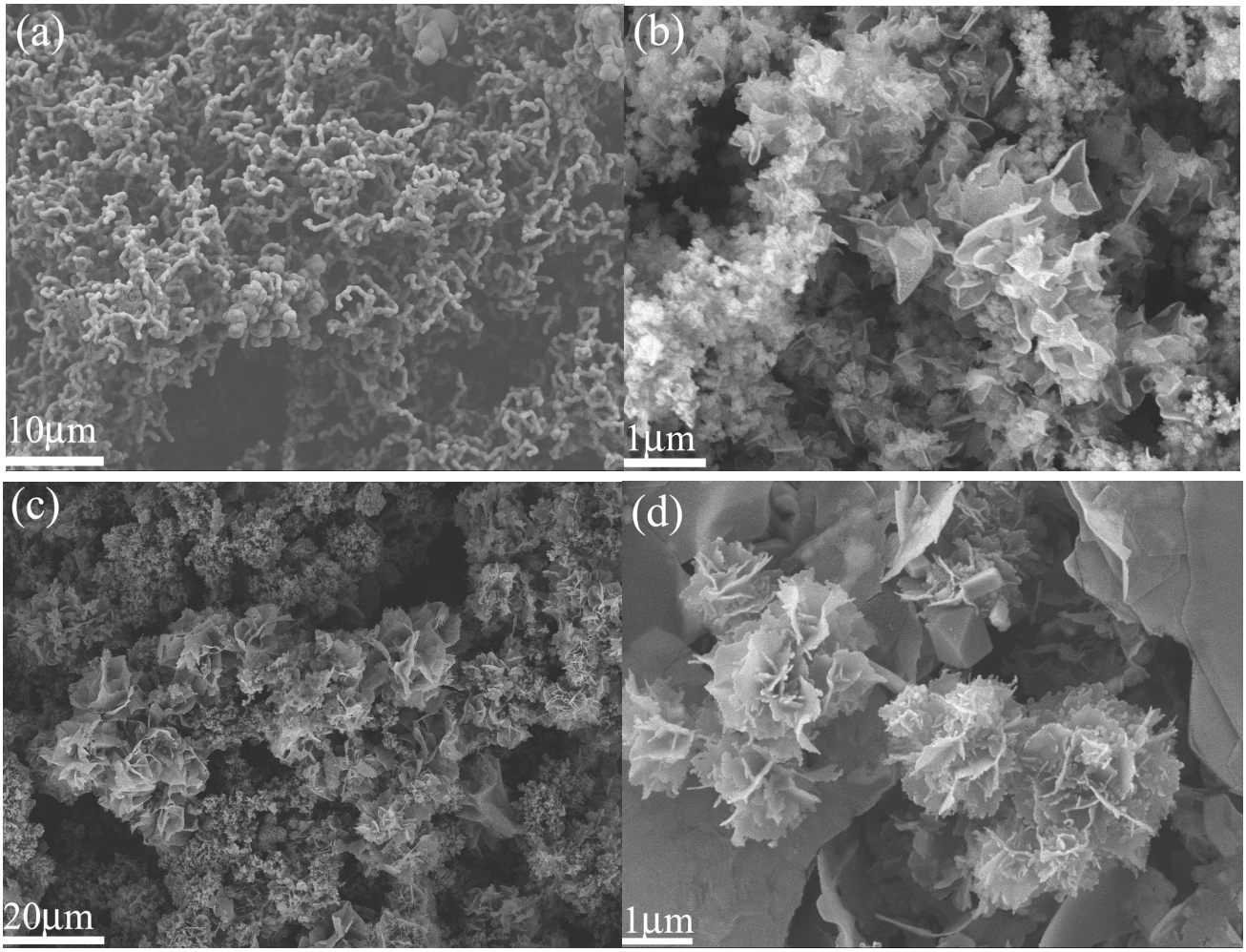

Fig. 8 (a) FESEM images of the products using H_2O replacing NaN_3; (b) FESEM images of the products using $NaNH_2$ replacing NaN_3; (c) FESEM images of the products using $CO(NH_2)_2$ replacing NaN_3; (d) FESEM images of the products using S powder replacing NaN_3.

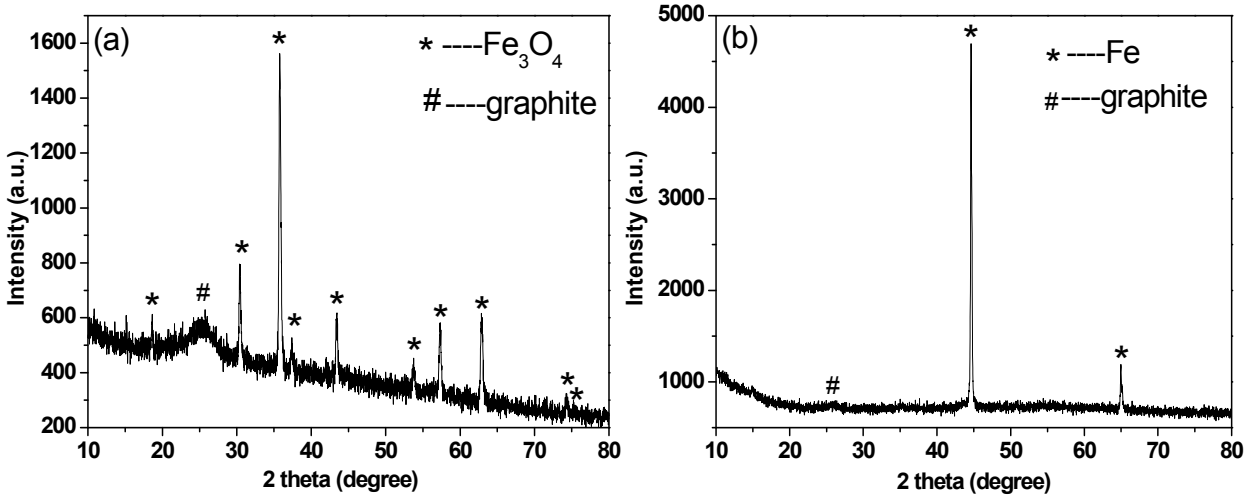

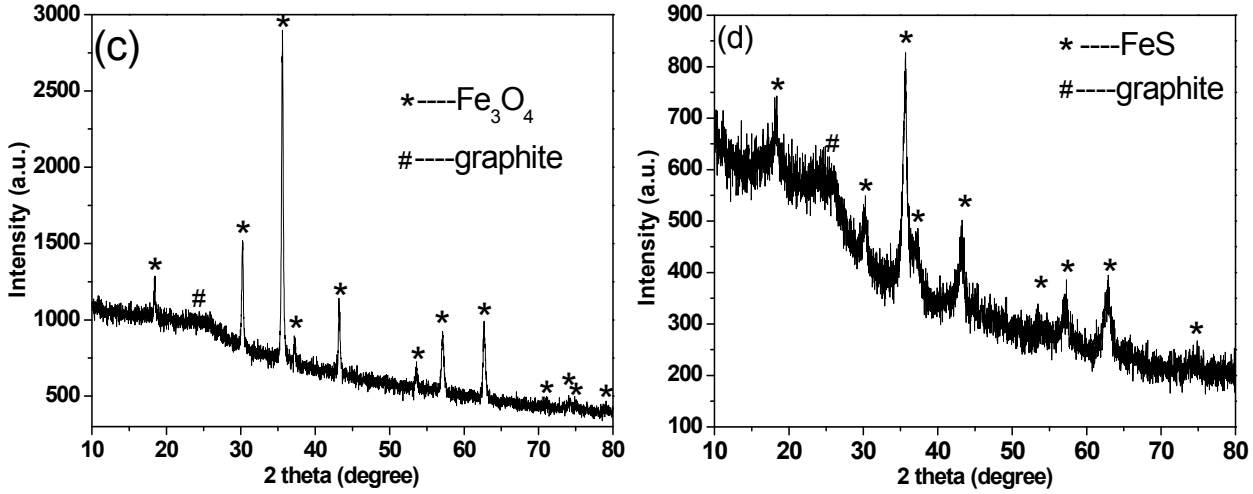

Fig. 9 (a) XRD pattern of the products using H_2O replacing NaN_3; (b) XRD pattern of the products using $NaNH_2$ replacing NaN_3; (c) XRD pattern of the products using $CO(NH_2)_2$ replacing NaN_3; (d) XRD pattern of the products using S powder replacing NaN_3.

The magnetic properties were investigated at room temperature with an applied field from -10000 Oe to 10000 Oe. In Fig. 10(b), the magnetic hysteresis loop of Fe/carbon nantotube nanocomposites at 600 °C shows ferromagnetic behavior with saturation magnetization (*Ms*), remanent magnetization (*Mr*), and coercivity (*Hc*) values of ca. 62.7 emu/g, 6.7 emu/g and 187.3 Oe. Compared to those reported results elsewhere [39], the *Ms* value is smaller than the value of bulk Fe (212 emu/g). The decrease in the value of *Ms* found in this work might be most likely attributed to the wide existence of carbon nanotubes, and these carbon nanotubes restrict the optional movement and interactions of the α-Fe nanoparticles. Its role is similar to that of the surfactant that existed on the Fe nanoparticles, which leads to decrease *Ms* value [40]. This may be also attributed to small size of Fe nanoparticles (~30 nm). The results of burring experiments indicate that the calculated Fe to Fe/ carbon nanotube nanocomposites mass ratio of the products is about 0.3065. Additionally, Fig. 10(a) and 10(c) show that the saturation magnetizations (*Ms*) of Fe/ carbon nanotube nanocomposites at 500 °C and 700 °C are ca. 60.9 emu/g and 64.9 emu/g, which are similar to the value of Fe/ carbon nanotube nanocomposites at 600 °C. However, the *Hc* values of Fe/ carbon nanotube

nanocomposites at 500 °C and 700 °C are ca. 114.2 Oe and 87.0 Oe, which are smaller than the value (187.3 Oe) of Fe/ carbon nanotube nanocomposites at 600 °C. The reason for high H_c value of Fe/carbon nanotube nanocomposites at 600 °C might result from the high content quasi-one-dimensional arrangement of magnetic nanoparticles by the restriction of carbon nanotubes [41]. Moreover, it was observed that the obtained sample showed no change in magnetic properties after being kept in air for over two months, suggesting that the α-Fe nanoparticles were well protected by the graphite layers.

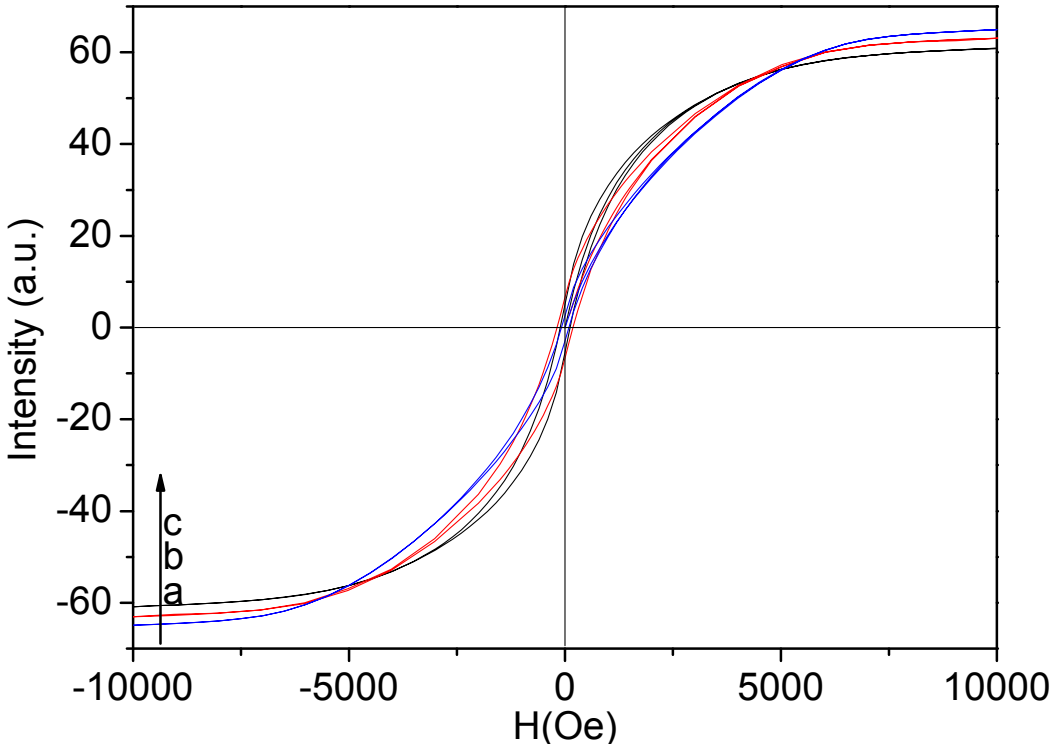

Fig. 10 Magnetic hysteresis loops of Fe/carbon nanotube nanocomposites at room temperature: (a) 500 °C; (b) 600 °C; (c) 700 °C.

4. Conclusions

In summary, Fe/carbon nanotube nanocomposites with sponge-like structures were synthesized through catalytic decomposition of waste PP at 600 °C. The Fe/C nanocomposites were mainly

self-assembled by carbon nanotubes and Fe nanoparticles due to magnetic interaction. The diameter of carbon nanotubes is about 30 nm and the diameter of Fe nanoparticles in carbon nanotubes is also about 30 nm. The BET surface area is calculated to be 197.6 m^2/g, and the BJH adsorption cumulative volume of pores is up to 0.2860 cm^3/g. Magnetic hysteresis loop measurement shows that the sponge-like Fe/carbon nanotube nanocomposites display ferromagnetic properties at room temperature, and the saturation magnetization value (62.7 emu/g) is lower than that of bulk Fe, which can be attributed to the wide existence of carbon nanotubes and the reduced size of Fe nanoparticles. The high coercivity (*Hc*) value (187.3 Oe) might result from the high content quasi-one-dimensional arrangement of magnetic nanoparticles by the restriction of carbon nanotubes.

Acknowledgment

The work was financially supported by Natural Science Foundation of Jiangsu Province (No. BK20141293, BK2012276), Natural Science Foundation of the Higher Education Institutions of Jiangsu Province (No. 13KJB430012), the Opening Project of CAS Key Laboratory of Materials for Energy Conversion (No. KF 2014006), Natural Science Foundation of China (No. 51203069), and Qinglan project.

References

[1] C. Yu, Y. Sun, X. M. Fan, Z. B. Zhao, J. S. Qiu. Part. Part. Syst. Char., 2013, **30**, 637.

[2] H. B. Geng, Q. Zhou, Y. Pan, H. W. Gu, J. W. Zheng. Nanoscale, 2014, **6**, 3889.

[3] I. A. Choi, Y. Li , D. J. Kim, M. Pal, J. H. Cho, K. Lee, M. H. Jung, C. Lee, W. S. Seo. Chem. Asian J., 2013, **8**, 290.

[4] X. W. Wei, G. X. Zhu, C. J. Xia, Y. Ye. Nanotechnology, 2006, **17**, 4307.

[5] W. S. Seo, J. H. Lee, X. M. Sun, Y. Suzuki, D. Mann, Z. Liu, M. Terashima, P. C. Yang, M. V. McConnell, D. G. Nishimura, H. J. Dai. Nat. Mater., 2006, **5**, 971.

[6] X. J. Fan, G. Z. Jiao, L. Gao, P. F. Jin, X. Li. J. Mater. Chem. B, 2013, **1**, 2658.

[7] G. G. Liu, F. He, J. Zhang, L. J. Li, F. J. Li, L. X. Chen, Y. Huang. Appl. Catal. B-Environ., 2014, **150**, 515.

[8] Z. X. Wu, W. Li, P. A. Webley, D. Y. Zhao. Adv. Mater., 2012, **24**, 485.

[9] Y. Yang, Z. Guo, H. Zhang, D. Q. Huang, J. L. Gu, Z. H. Huang, F. Y. Kang, T. A. Hatton, G. C. Rutledge. J. Appl. Polym. Sci., 2013, **127**, 4288.

[10] X. Zhang, O. Allou, J. H. Zhu, Q. L. He, Z. P. Luo, H. A. Colorado, N. Haldolaarachchige, D. P. Young, T. D. Shen, S. Y. Wei, Z. H. Guo. RSC Adv., 2013, **3**, 9453.

[11] T. Ren, Y. Si, J. M. Yang, B. Ding, X. X. Yang, F. Hong, J. Y. Yu. J. Mater. Chem., 2012, **22**, 15919.

[12] N. Aguiló-Aguayo, Z. Y. Liu, E. Bertran, J. Yang. J. Phys. Chem. C, 2013, **117**, 19167.

[13] C. N. He, S. Wu, N. Q. Zhao, C. S. Shi, E. Z. Liu, J. J. Li. ACS Nano, 2013, **7**, 4459.

[14] M. del. C. Gimenez-Lopez1, A. L. Torre1, M. W. Fay, P. D. Brown, A. N. Khlobystov1. Angew. Chem. Int. Edit., 2013, **52**, 2051.

[15] P. Lukanov, V. K. Anuganti, Y. Krupskaya, A. M. Galibert, B. Soula, C. Tilmaciu, A. H. Velders, R. Klingeler, B. Büchner, E. Flahaut. Adv. Funct. Mater., 2011, **21**, 3583.

[16] H. Y. Niu, Y. X. Wang, X. L. Zhang, Z. F. Meng, Y. Q. Cai. ACS Appl. Mater. Interfaces, 2012, **4**, 286.

[17] A. Zhypargul, O. Emil, I. Chihiro, S. G. Hullathy, S. Saadat, L. L. Chen, M. Tsutomu. Carbon, 2012, **50**, 1776.

[18] Z. X. Wu, W. Li, P. A. Webley, D. Y. Zhao. Adv. Mater., 2012, **24**, 485.

[19] M. Bystrzejewski, O. Labedz, W. Kaszuwara, A. Huczko, H. Lange. Powder Technol., 2013, **246**, 7.

[20] H. J. Lee, W. Cho, E. Lim, M. Oh. Chem. Commun., 2014, **50**, 5476.

[21] D. P. Serrano, J. Aguado, J. M. Escola. ACS Catal., 2012, **2**, 1924.

[22] C. W. Zhuo, Y. A. Levendis. J. Appl. Polym. Sci., 2014, **131**, 39931.

[23] C. F. Wu, Z. C. Wang, L. Z. Wang, P. T. Williams, J. Huang. RSC Adv., 2012, **2**, 4045.

[24] J. N. Sahu, K. K. Mahalik, H. K. Nam, T. Y. Ling, T. S. Woon, M. S. B. Rahman, Y. K. Mohanty, N. S. Jayakumar, S. S. Jamuar. Environ. Prog. Sustain. Energy, 2014, **33**, 298.

[25] P. A. Wager, M. Schluep, E. Muller, R. Gloor. Environ. Sci. Technol., 2012, **46**, 628.

[26] N. Fraunholcz. Miner. Eng., 2004, **17**, 261.

[27] H. S. Park, C. G. Kim, S. J. Kim. J. Ind. Eng. Chem.**,** 2006, **12**, 216.

[28] S. K. Ouiminga, T. Rogaume, M. Sougoti, J. M. Commandre, J. Koulidiati. J. Anal. Appl. Pyrolysis, 2009, **86**, 260.

[29] S. H. Jung, M. H. Cho, B. S. Kang, J. S. Kim. Fuel Process Technol., 2010, **91**, 277.

[30] A. H. Lu, W. C. Li, E. L. Salabas, B. Spliethoff, F. Schuth. Chem. Mater.**,** 2006, **18**, 2086.

[31] M. T. Kartel, N. V. Sych, M. M. Tsyba, V. V. Strelko. Carbon, 2006, **44**, 1019.

[32] C. F. Wu, M. A. Nahil, N. Miskolczi, J. Huang, P. T. Williams. Environ. Sci. Technol., 2014, **48**, 819.

[33] J. C. Acomb, C. F. Wu, P. T. Williams. Appl. Catal. B-Environ., 2014, **147**, 571.

[34] S. Y. Sawant, R. S. Somani, A. B. Panda, H. C. Bajaj. ACS Sustain. Chem. Eng., 2013, **1**, 1390.

[35] J. H. Zhang, B. Yan , S. Wan, Q. H. Kong. Ind. Eng. Chem. Res., 2013, **52**, 5708.

[36] J. A. Onwudili, N. Insura, P. T. Williams. J. Energy Inst., 2013, **86**, 227.

[37] J. H. Zhang, B. Yan, H. Wu, Q. H. Kong. RSC Adv., 2014, **4**, 6991.

[38] J. H. Zhang, J. Du, Y. T. Qian, S. L. Xiong. Mater. Res. Bull., 2010, **45**, 15.

[39] Y. Leconte, S. Veintemillas-Verdaguer, M. P. Morales, R. Costo, I. Rodriguez, P. Bonville, B. Bouchet-Fabre, N. Herlin-Boime. J. Colloid Interface Sci., 2007, **313**, 511.

[40] S. Ghosh, W. Jiang, J. D. Mcclements, B. S. Xing. Langmuir, 2011, **27**, 8036.

[41] F. Zhao, H. Y. Duan, W. G. Wang, J. Wang. Physica B, 2012, **407**, 2495.